Available online at www.CivileJournal.org

Civil Engineering Journal

(E-ISSN: 2476-3055; ISSN: 2676-6957)

Vol. 8, No. 10, October, 2022

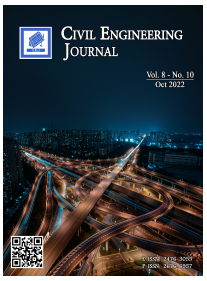

A Triangular Shell Element Based on Higher-order Strains for the Analysis of Static and Free Vibration

Hamida Sekkour [1*], Lamine Belounar [1], Abderahim Belounar [2], Faiçal Boussem [3], Lahcene Fortas [1]

[1] *NMISSI Laboratory, Biskra University, BP145 Biskra 07000, Algeria.*

[2] *Department of Civil Engineering, University Center of Tipaza, Tipaza, Algeria.*

[3] *Department of Hydrocarbons and Renewable Energies, Adrar University, Algeria.*

Received 15 May 2022; Revised 10 September 2022; Accepted 23 September 2022; Published 01 October 2022

Abstract

This research paper proposes a new triangular cylindrical finite element for static and free vibration analysis of cylindrical structures. The formulation of the proposed element is based on deep shell theory and uses assumed strain functions instead of displacement functions. The assumed strain functions satisfy the compatibility equations. This finite element possesses only the five necessary degrees of freedom for each of the three corner nodes. The element's displacement field, which contains higher-order terms, satisfies the requirement of rigid-body displacement. The element's performance is evaluated using various numerical static and free vibration tests for cylindrical shell problems, including an analysis of the effect of shell openings on natural frequencies. The results of the developed element are evaluated in comparison with published analytical and numerical solutions. The new cylindrical element's formulation is straightforward. Compared to the degenerate nine-node shell element and other elements, the results of the present element have shown excellent accuracy and efficiency in predicting static and free vibration of curved structures. This element only requires the use of very coarse meshes to converge. In addition, the triangular shape of this element is more advantageous than the quadrilateral shape when the geometric domain of the structure is deformed or complicated.

Keywords: Strain Approach; Curved Structures; Deep Shells Theory; Cylindrical Finite Element; Free Vibration.

1. Introduction

The numerical analysis of shell structures is often used to solve problems in engineering and industry. The finite element method is one of the popular methods used by researchers to simulate the behavior of curved structures [1]. Three types of finite elements are employed: first, the curved shell elements derived from general shell theory, such as Zienkiewicz [2], and Liang & Izzuddin [3]; Second, degenerated shell elements that were obtained from the three-dimensional solid theory, as Abed-Meraim & Combescure [4] and Trinh et al. [5]; third, an approximate representation of the geometry by flat shell elements [6–8]. However, the necessity of using curved shell elements offers numerous advantages, as demonstrated by Jones & Strome [9]: Deriving structural stiffness equations does not involve any additional geometric approximations or coordinate transformations. In addition, using curved shell elements produces efficient elements and avoids problems such as slow convergence for strongly curved shells.

Therefore, the formulation of curved shell elements has received more attention, such as the rectangular element developed by Connor & Brebbia [10] and Cantin & Clough [11]. This cylindrical shell element had better responses

* Corresponding author: hamidasekkour@yahoo.fr

http://dx.doi.org/10.28991/CEJ-2022-08-10-06

for coarse meshes when the cylindrical shell was tested. The higher-order elements [12–14] are developed using the displacement formulation with additional degrees of freedom. There are also other works based on three-dimensional elements, such as the 20-node solid element for shell analysis [15] and the 3D finite element (SFR8) based on the space fiber rotation concept (SFR) developed by Ayad et al. [16]. However, the overall structural matrix has a substantially wider bandwidth when higher-order finite elements with more degrees of freedom are used. Furthermore, there is no link between the additional internal degrees of freedom and the associated generalized physical forces. This work has therefore given priority to the development of higher-order curved elements with only the necessary degrees of freedom.

The employment of finite elements based on assumed strain functions has provided several advantages [17], including the simplicity of satisfying the convergence criteria (constant deformations and rigid body motion). In addition, these independent assumed strains satisfy the compatibility equations, as well as the ability to have the displacement field reinforced by high-order terms without adding intermediate nodes or non-essential degrees of freedom. The strain approach was applied to develop finite elements in which imposed strains were proposed, and the corresponding displacement functions were obtained by simple integration of the strain-displacement relations. A brief review of the strain approach found in the literature for different elements is presented as follows. This approach was applied for isotropic plate bending analysis [17–22], functionally graded plates [23, 24], composite plate materials [25], general plane elasticity problems [26–29], and three-dimensional analysis [30–34].

The contribution of the strain approach for curved shell elements has been shown by the formulation of the first cylindrical shell element based on deep shell theory [35]. This element has only five necessary external nodal degrees of freedom per node and is rectangular in plan. From the validation tests, this element shows superior convergence with coarse mesh compared to all other rectangular elements. Based on the shallow shell theory, several rectangular, cylindrical shell elements were formulated by Djoudi & Bahai [36-38]. The first was used for linear and geometric non-linear analysis. The second element was used to study how cut-outs affected the vibration behaviors of cylindrical panels, and the last element was used to calculate the natural frequencies of cylindrical panels. To improve the performance of strain-based finite shell elements, Bourezane [39] proposed a rectangular, cylindrical shell element with six degrees of freedom per node by introducing an additional rotational degree of freedom. The effectiveness of these elements was demonstrated, and an acceptable degree of accuracy was reached without using many elements. Therefore, all the cylindrical shell elements [35-39] based on the strain approach presented above are rectangular. The reasons mentioned above prompted the authors to use this approach to develop a new triangular cylindrical shell element.

In this research, a three-node triangular cylindrical shell element has been developed to analyze curved structures using the strain approach and deep shell theory. Only five degrees of freedom are used per node for the developed element called SBTDS (Strain Based Triangular Deep shell). This element is based on assumed strains satisfying the compatibility equations and the rigid body modes for displacements. Numerical integration has been used for calculating the element stiffness and mass matrices. Various examples of static and free vibration of curved structures were used to evaluate the results of the element (SBTDS), and the results then compared to previously published solutions.

2. Theoretical Considerations

Consider the curved triangular element shown in Figure 1. The center (O) of the hypotenuse of the element is the origin of the curvilinear coordinates x, y, and z ($y=R\varphi$). The present element is formulated using deep shell theory, and the strain displacement equations in a system curvilinear coordinates are given [35].

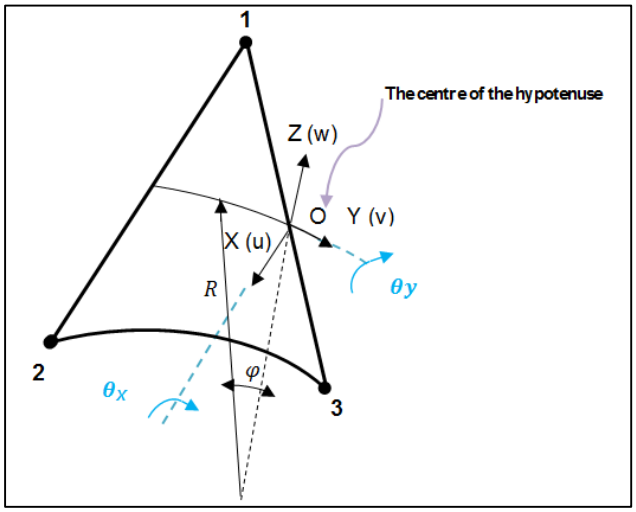

Figure 1. Triangular cylindrical deep shell element (SBTDS)

$$\varepsilon_x = \frac{\partial U}{\partial x}, \varepsilon_\varphi = \frac{1}{R}\frac{\partial V}{\partial \varphi} + \frac{W}{R}, \gamma_{x\varphi} = \frac{1}{R}\frac{\partial U}{\partial \varphi} + \frac{\partial V}{\partial x}$$
$$k_x = -\frac{\partial^2 W}{\partial x^2}, k_\varphi = \frac{1}{R^2}\frac{\partial V}{\partial \varphi} - \frac{1}{R^2}\frac{\partial^2 W}{\partial \varphi^2}, k_{x\varphi} = \frac{1}{R}\frac{\partial V}{\partial x} - \frac{1}{R}\frac{\partial^2 W}{\partial x \partial \varphi} \quad (1)$$

As the displacements, U, V, and W are used to represent the six deformations given in Equation 1, these displacements have to verify the compatibility equations written as follows:

$$\frac{\partial^2 \varepsilon_\varphi}{\partial x^2} + \frac{k_x}{R} + \frac{1}{R^2}\frac{\partial^2 \varepsilon_x}{\partial \varphi^2} - \frac{1}{R}\frac{\partial^2 \gamma_{x\varphi}}{\partial x \partial \varphi} = 0, \frac{\partial k_{x\varphi}}{\partial x} - \frac{1}{R}\frac{\partial k_x}{\partial \varphi} + \frac{1}{R^2}\frac{\partial \varepsilon_x}{\partial \varphi} - \frac{1}{R}\frac{\partial \gamma_{x\varphi}}{\partial x} = 0$$
$$\frac{\partial k_\varphi}{\partial x} - \frac{1}{R}\frac{\partial k_{x\varphi}}{\partial \varphi} = 0 \quad (2)$$

The displacement modes of rigid bodies are determined by equating Equation 1 to zero, and then after integration, the following displacement fields, U, V, and W, are calculated:

$$U = R\alpha_2 \cos\varphi + R\alpha_4 \sin\varphi + \alpha_5$$
$$V = (\alpha_1 + \alpha_2 x)\sin\varphi - (\alpha_3 + \alpha_4 x)\cos\varphi + \alpha_6 \quad (3)$$
$$W = -(\alpha_1 + \alpha_2 x)\cos\varphi - (\alpha_3 + \alpha_4 x)\sin\varphi$$

This element has five degrees of freedom $\left(U, V, W, \theta_y = \frac{\partial W}{\partial x}, \theta_x = \frac{\partial W}{R\partial \varphi} - \frac{V}{R}\right)$ at each of the three nodes. Moreover, hence the displacement functions should contain only 15 constants where six constants (α_1, α_2,……α_6) having used for the rigid body modes, and the remaining constants (α_7, α_8,…… α_{15}) are distributed among the six suggested strains in the following manner:

$$\varepsilon_x = \alpha_7, \quad \varepsilon_\varphi = \alpha_8 + [-\frac{1}{2R}\alpha_{10}x^2 - \frac{1}{6R}\alpha_{11}x^3 - \frac{1}{6R^2}\alpha_{12}x^3 y]$$
$$\gamma_{x\varphi} = \alpha_9, \quad k_x = \alpha_{10} + \alpha_{11}x + \frac{1}{R}\alpha_{12}xy \quad (4)$$
$$k_\varphi = \alpha_{13} + \frac{y}{R}\alpha_{14}, \quad k_{x\varphi} = \alpha_{15} + \left[\frac{\alpha_{12}}{2R}x^2\right]$$

The terms for the assumed strains in brackets (Equation 4) must be added to verify the compatibility equations (Equation 2). Then, the strain functions expressed in Equation 4 are replaced in Equation 1, and the displacement functions that are obtained after integration are added to the corresponding expressions in Equation 3 to obtain the complete displacement functions:

$$U = R\alpha_2 \cos\varphi + R\alpha_4 \sin\varphi + \alpha_5 + x\alpha_7 + y\alpha_9 - Ry\alpha_{15}$$
$$V = (\alpha_1 + \alpha_2 x)\sin\varphi - (\alpha_3 + \alpha_4 x)\cos\varphi + \alpha_6 + Ry\alpha_{13} + \frac{y^2}{2}\alpha_{14} + Rx\alpha_{15}$$
$$W = -(\alpha_1 + \alpha_2 x)\cos\varphi - (\alpha_3 + \alpha_4 x)\sin\varphi + R\alpha_8 - \frac{x^2}{2}\alpha_{10} - \frac{x^3}{6}\alpha_{11} - \frac{yx^3}{6R}\alpha_{12} - R^2\alpha_{13} - Ry\alpha_{14} \quad (5)$$
$$\theta_x = -\frac{1}{R}\alpha_6 - \frac{x^3}{6R}\alpha_{12} - \alpha_{13}y - (R + \frac{y^2}{2R})\alpha_{14} - x\alpha_{15}$$
$$\theta_y = -\alpha_2 \cos\varphi - \alpha_4 \sin\varphi - x\alpha_{10} - \frac{x^2}{2}\alpha_{11} - \frac{yx^2}{2R}\alpha_{12}$$

Equations 4 and 5 describing the element's displacement and strain functions are written in matrix form, respectively.

$$\{U\} = [P]\{\alpha\} \quad (6)$$

$$\{\varepsilon\} = [Q]\{\alpha\} \tag{7}$$

with $\{\alpha\}=\{\alpha_1, \alpha_2, \dots, \alpha_{15}\}^T$; where the matrices $[P]$ and $[Q]$ are defined as follows:

$$[P]=\begin{bmatrix} 0 & R\cos\varphi & 0 & R\sin\varphi & 1 & 0 & x & 0 & y & 0 & 0 & 0 & 0 & 0 & -Ry \\ \sin\varphi & x\sin\varphi & -\cos\varphi & -x\cos\varphi & 0 & 1 & 0 & 0 & 0 & 0 & 0 & 0 & Ry & \frac{y^2}{2} & Rx \\ -\cos\varphi & -x\cos\varphi & -\sin\varphi & -x\sin\varphi & 0 & 0 & 0 & R & 0 & -\frac{x^2}{2} & -\frac{x^3}{6} & -\frac{yx^3}{6R} & -R^2 & -Ry & 0 \\ 0 & 0 & 0 & 0 & 0 & -\frac{1}{R} & 0 & 0 & 0 & 0 & 0 & -\frac{x^3}{6R} & -y & -\left(R+\frac{y^2}{2R}\right) & -x \\ 0 & -\cos\varphi & 0 & -\sin\varphi & 0 & 0 & 0 & 0 & 0 & -x & -\frac{x^2}{2} & -\frac{yx^2}{2R} & 0 & 0 & 0 \end{bmatrix} \tag{8}$$

$$[Q] = \begin{bmatrix} 0 & 0 & 0 & 0 & 0 & 0 & 1 & 0 & 0 & 0 & 0 & 0 & 0 & 0 & 0 \\ 0 & 0 & 0 & 0 & 0 & 0 & 0 & 1 & 0 & -\frac{x^2}{2R} & -\frac{x^3}{6R} & -\frac{yx^3}{6R^2} & 0 & 0 & 0 \\ 0 & 0 & 0 & 0 & 0 & 0 & 0 & 0 & 1 & 0 & 0 & 0 & 0 & 0 & 0 \\ 0 & 0 & 0 & 0 & 0 & 0 & 0 & 0 & 0 & 1 & x & \frac{xy}{R} & 0 & 0 & 0 \\ 0 & 0 & 0 & 0 & 0 & 0 & 0 & 0 & 0 & 0 & 0 & 0 & 1 & \frac{y}{R} & 0 \\ 0 & 0 & 0 & 0 & 0 & 0 & 0 & 0 & 0 & 0 & 0 & \frac{x^2}{2R} & 0 & 0 & 1 \end{bmatrix} \tag{9}$$

The element nodal displacements vector $\{q_e\}$ is connected to the vector of constants by the transformation matrix [C], which is given in the Appendix I, as follows:

$$\{q_e\} = [C]\{\alpha\} \tag{10}$$

Equation 10 can be used to derive the constant parameters vector $\{\alpha\}$ as follows:

$$\{\alpha\} = [C]^{-1}\{q_e\} \tag{11}$$

Equation 11 is substituted for Equations 6 and 7 to produce the following result:

$$\{U\} = [P][C]^{-1}\{q_e\} = [N]\{q_e\} \tag{12}$$

$$\{\varepsilon\} = [Q][C]^{-1}\{q_e\} = [B]\{q_e\} \tag{13}$$

With;

$$[N] = [P][C]^{-1}; [B] = [Q][C]^{-1} \tag{14}$$

By using the conventional expression, the stiffness and mass matrices ($[K^e]$, $[M^e]$) may be derived, respectively:

$$\left[K^e\right] = \int_{V_e} [B]^T [D][B] dV = [C]^{-T} \underbrace{\left(\frac{1}{2}\int [Q]^T [D][Q] \det(J) d\xi d\eta\right)}_{[K_0]} [C]^{-1} \tag{15}$$

$$\left[M^e\right] = \rho h \int_{S_e} [N]^T [N] dS = [C]^{-T} \underbrace{\left(\frac{1}{2}\rho h \int [P]^T [P] \det(J) d\xi d\eta\right)}_{[M_0]} [C]^{-1} \tag{16}$$

where, [D], $[D_m]$ and $[D_b]$ are, respectively, matrices of rigidity, membrane rigidity, and bending rigidity.

$$[D]=\begin{bmatrix} [D_m] & 0 \\ 0 & [D_b] \end{bmatrix}, \quad [D_m] = \frac{Eh}{1-\nu^2}\begin{bmatrix} 1 & 0 & 0 \\ 0 & 1 & 0 \\ 0 & 0 & \frac{1-\nu}{2} \end{bmatrix}, \quad [D_b] = \frac{Eh^3}{12\left(1-\nu^2\right)}\begin{bmatrix} 1 & 0 & 0 \\ 0 & 1 & 0 \\ 0 & 0 & \frac{1-\nu}{2} \end{bmatrix} \tag{17}$$

The matrices [K_0] and [M_0] given in Equations 15 and 16 are computed numerically. The stiffness and mass matrices of the elements ([k^e] and [M^e]) are then obtained. They are then assembled to calculate the stiffness and mass matrices of the structure ([K and [M]). And then, the following equations are used for the static analysis and the free vibration analysis, respectively.

$$[K]\{q\} = \{F\} \tag{18}$$

$$\left([K] - \omega^2[M]\right)\{q\} = 0 \tag{19}$$

where {q} and {F} are respectively structural nodal displacements and structural nodal forces vectors whereas ω is the angular frequency.

3. Numerical Validation

To evaluate the accuracy and efficiency of the formulated element (SBTDS), several numerical examples of static and free vibration analysis are examined.

3.1. Static Analysis

3.1.1. Square Pinched Cylinder with Free Edges

The pinched cylinder illustrated in Figure 2 is the first problem to be solved. The literature frequently uses this test case as one example to evaluate finite elements' convergence. Only one-eighth of the cylinder is modelized with a variety of meshes for reasons of symmetry (Figure 3); the geometrical, mechanical characteristics, boundary, and symmetry conditions are represented in Figure 2, where two cases can be distinguished for the cylinder thickness and applied loads. Tables 1 and 2 show the normal displacement results W_C at point C, which illustrate the high precision obtained by the present element. The results of the developed element are similar to the analytical solution [40]. However, a divergence of results is observed for the Djoudi element, which is based on the shallow shell theory (Figure 4).

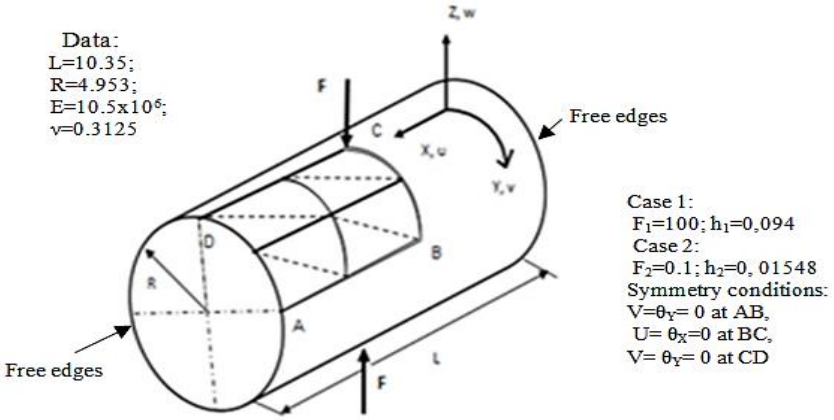

Figure 2. Pinched cylinder with free edges

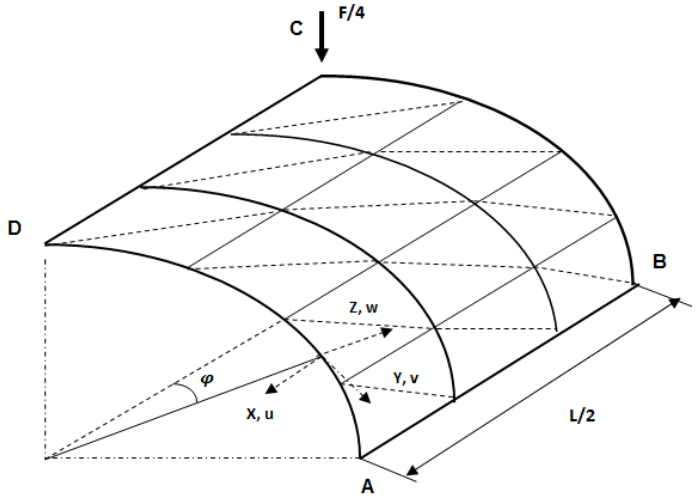

Figure 3. Meshes of pinched cylinder with free edges

Table 1. Convergence of displacement W_C of a pinched cylinder with free edges, Case 1: F_1=100; h_1=0,094

Mesh	ASH element	Djoudi element *	Present element (SBTDS)
2×2	0.1104	0.0641	0.1076
4×4	0.1132	0.0662	0.1134
6×6	0.1138	0.0667	0.1136
8×8	0.1140	0.0669	0.1139
10×10	0.1141	0.0669	0.1143
Ref. solution [40]			0.1139

* The results were obtained by using Djoudi element formulation [36].

Table 2. Convergence of displacement W_C of a pinched cylinder with free edges, Case 2: F_2=0.1; h_2=0, 01548

Mesh	ASH element	Djoudi element*	Present element (SBTDS)
1×4	0.02431	0.01409	0.0243
2×2	0.02330	0.01406	0.0239
2×4	0.02437	0.01415	0.0244
2×8	0.02442	0.01420	0.0268
3×4	0.02443	0.01418	0.0243
4×4	0.02448	0.01420	0.0242
6×6	0.02456	0.01427	0.0247
Ref. solution [37]			0.02439

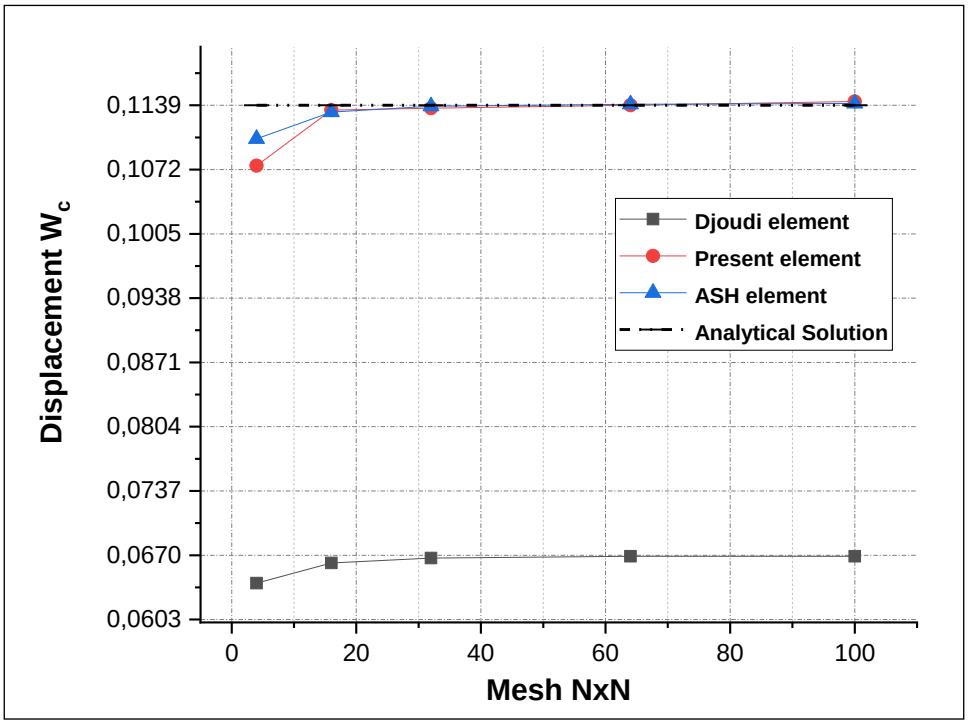

Figure 4. Convergence of displacement W_C of a pinched cylinder with free edges, Case 1: F_1=100; h_1=0,094

3.1.2. Curved Cantilever Beam

The second example is the curved cantilever beam clamped at one end and loaded at the other free end (Figure 5). The geometrical parameters and the values of Poisson's ratio, Young modulus, and load are shown in Figure 5. The results obtained for the deflection at the z-direction (Table 3) are compared with the theoretical solution given by Macneal & Harder [41] and with other finite elements [35, 36, 42]. Figure 6 shows the convergence of deflection at the z-direction for the curved beam. The proposed element (SBTDS) gives excellent results even for a small number of elements. The reference solution is reached by this element for a 1×4 mesh (Figure 6). Figure 6 shows that the SBTDS element produces more accurate results than those given by Djoudi element [36].

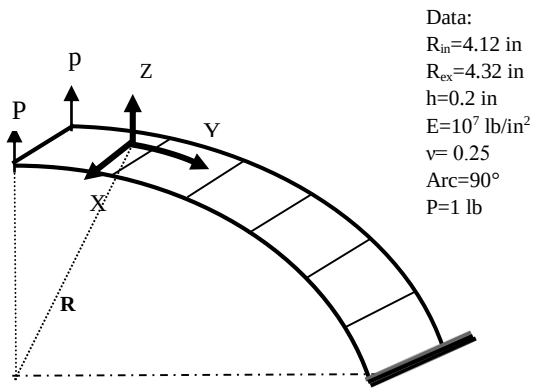

Figure 5. Curved cantilever beam with static loads

Table 3. Convergence of deflection at z-direction for curved beam

Mesh	ASH element	SAB element **	Djoudi element	Present element (SBTDS)
1×6	0.0880	0.0848	0.0626	0.0879
Ref. solution [38]			0.0886	

** The results were obtained by using SAB element formulation [39].

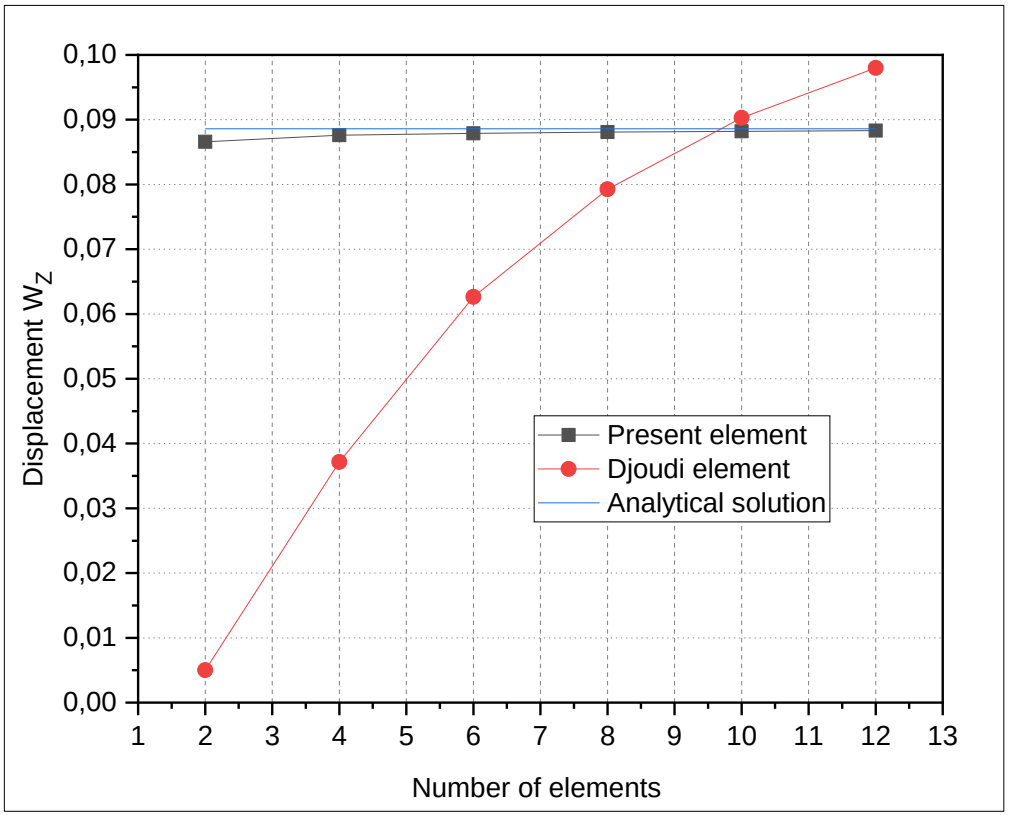

Figure 6. Convergence of deflection at z-direction for Curved Beam

3.1.3. Clamped Cylindrical Shell with Rigid Diaphragm

A different test case is a cylindrical shell clamped with a rigid diaphragm under two opposing concentrated loads. The performance of the shell elements in simulating complex membrane state problems dominated by bending is evaluated in this test. The geometrical, mechanical characteristics, loadings, boundary, and symmetry conditions are presented in Figure 7. One-eighth of the shell is considered for idealization. The results obtained for both the normal displacements at point C and tangential displacements at point *D* are compared with the theoretical solution [43] and with other finite elements CHA element [44]), ASH element [35], and Djoudi element [36]. The results of the SBTDS element (Table 4) are similar to those of the other elements. Graphical representations of these results are shown in Figures 8 and 9. The new triangular element (SBTDS) and the other rectangular elements give almost the same results for deflection.

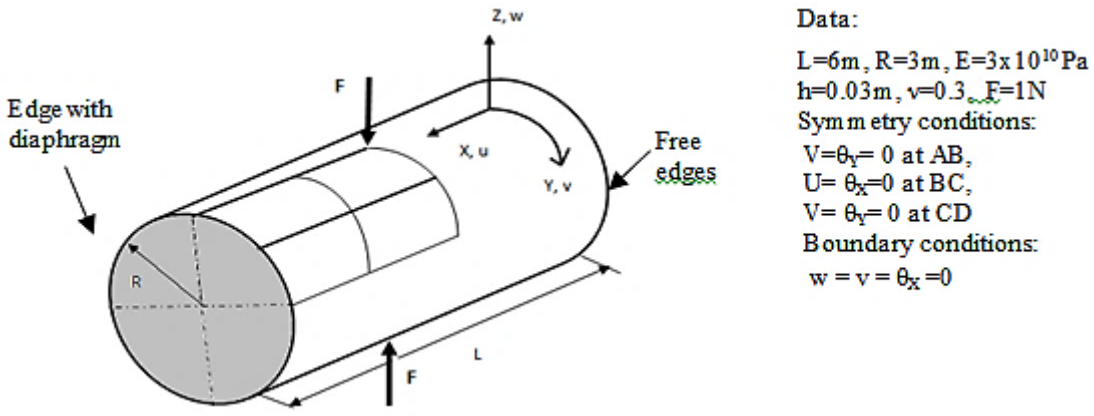

Figure 7. Pinched cylinder with a rigid diaphragm

Table 4. Convergence of tangential displacements at point (D)

Mesh	ASH element	CHA element [44]	Djoudi element	Present element (SBTDS)
2×2	3.356	3.114	3.484	0.603
4×4	5.173	5.087	4.878	3.663
6×6	4.570	4.541	4.294	4.040
8×8	4.392	4.377	4.116	4.049
10×10	4.314	4.304	4.036	4.087
12 × 12	4.273	4.266	3.995	4.122
14 × 14	4.244	4.239	3.968	4.148
Ref. solution [40]			4.114	

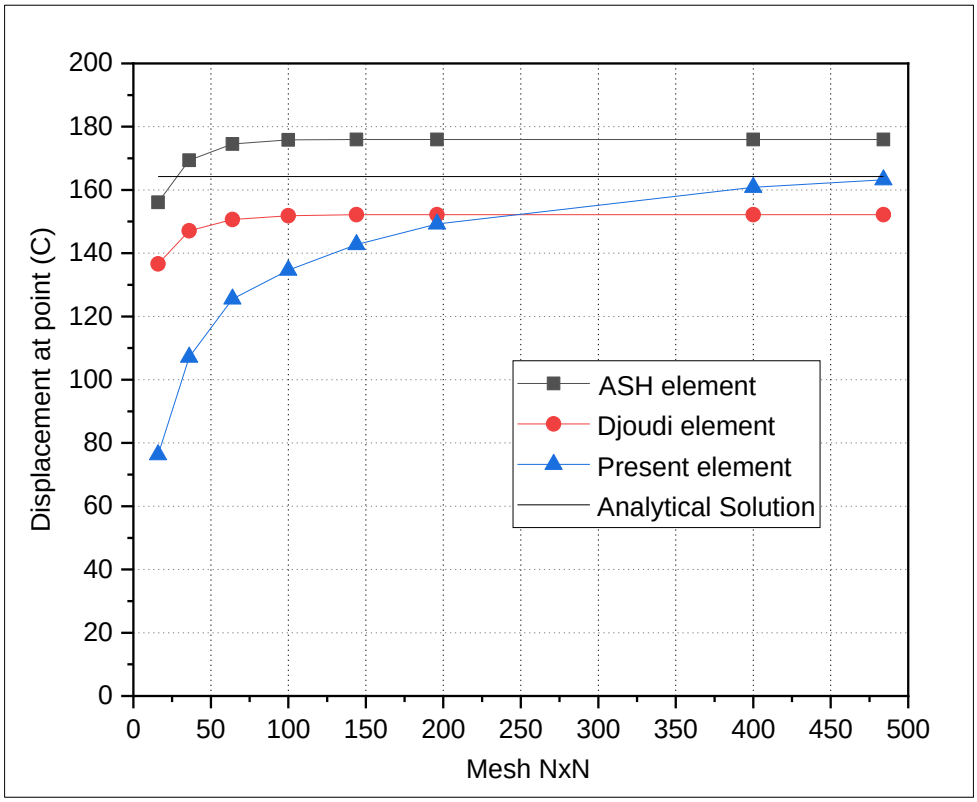

Figure 8. Convergence of normal displacement at point C

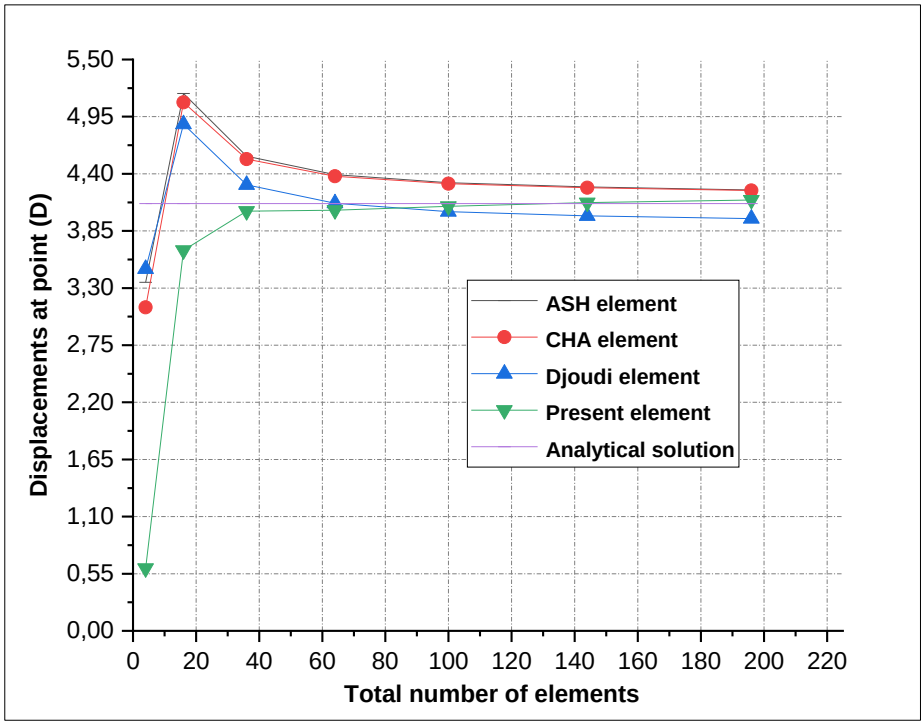

Figure 9. Convergence of normal displacement at point D

3.2. Free Vibration Analysis

3.2.1. Convergence of Mesh Discretization

In this test, we study the present element's convergence rate due to the domain discretization of a clamped cylindrical panel. The geometrical and mechanical characteristics of the panel are as follows: l = 1 m, r = 2 m, t = 0.005 m, φ=0.5 rad, Young's modulus $E = 208 \times 10^9$ N/m^2, Density ρ = 7833 kg/m^2, and Poisson's ratio is v = 0.29.

The results of the first and second natural frequencies are reported in Tables 5 and 6 against of the total number of elements and compared with the results of Djoudi element [37] and the theoretical solution [45]. In this test, we notice the high accuracy obtained by the present element, and its convergence to the theoretical solution is more rapid than that of Djoudi element [37].

Table 5. Convergence of the first natural frequencies of the clamped cylindrical panel and the relative errors

Mesh	Djoudi element [37]	Error (%)	Present element (SBTDS)	Error (%)
6×6	170.08	2.42	183.53	5.29
7×7	171.17	1.80	179.07	2.73
8×8	171.29	1.37	176.52	1.27
10×10	172.15	1.23	173.88	0.24

Table 6. Second natural frequencies of the clamped cylindrical panel and the relative errors

Mesh	Djoudi element [37]	Error (%)	Present element (SBTDS)	Error (%)
6×6	175.52	2.92	185.66	2.68
7×7	178.67	1.18	183.30	1.38
8×8	179.83	0.54	181.83	0.56
10×10	179.95	0.47	180.20	0.33

3.2.2. Clamped Cylindrical Panel

Another test case considered is a clamped cylindrical panel, and the geometry and material characteristics are illustrated in Figure 10. The results of the clamped panel frequencies obtained using a mesh of 10 ×10 are presented in Table 7 with analytical solution [46], numerical solution [47], and other finite elements, LAG9; nine-node shell element [48], ASL9; assumed strain shell element [49] and nine nodes degenerated shell element [50]. The frequencies obtained with the proposed element are better than those obtained with LAG9, ASL9, and the degenerate nine-node shell element, which is a very expensive element.

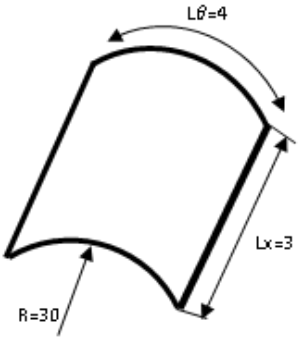

Figure 10. A clamped cylindrical panel (h = 0.013, E = 10^7, ρ = 0.096, v = 0.33)

Table 7. Natural frequencies of the clamped cylindrical panel

Mode	Analytical solution [46]	Numerical solution [47]	LAG9 [48]	ASL9 [49]	Nine node element [50]	Present element (SBTDS)
1	870	869.560	897.142	879.244	878.253	865.460
2	958	957.560	989.541	968.427	966.972	964.244

3.2.3 Effect of Central Openings on the Natural Frequencies of Cylindrical Panels

This example of cylindrical panels with a central opening (Figure 11) clamped along all four edges, treated by the Djoudi [35], is analyzed to study the effect of the openings on natural frequencies. The geometry and material properties of the panel are illustrated in Figure 11. Figure 12 compares the natural frequencies of the current element SBTDS to those of the Djoudi element [35]. It should be noted that the width of the hole has the same impact on the natural frequency for both elements and that the current element's numerical results agree with the Djoudi element's result.

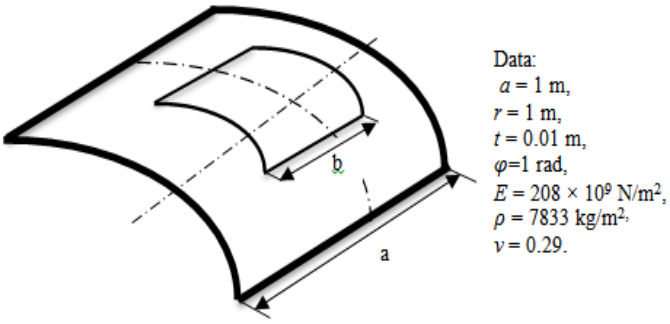

Figure 11. Cylindrical panels with a central opening

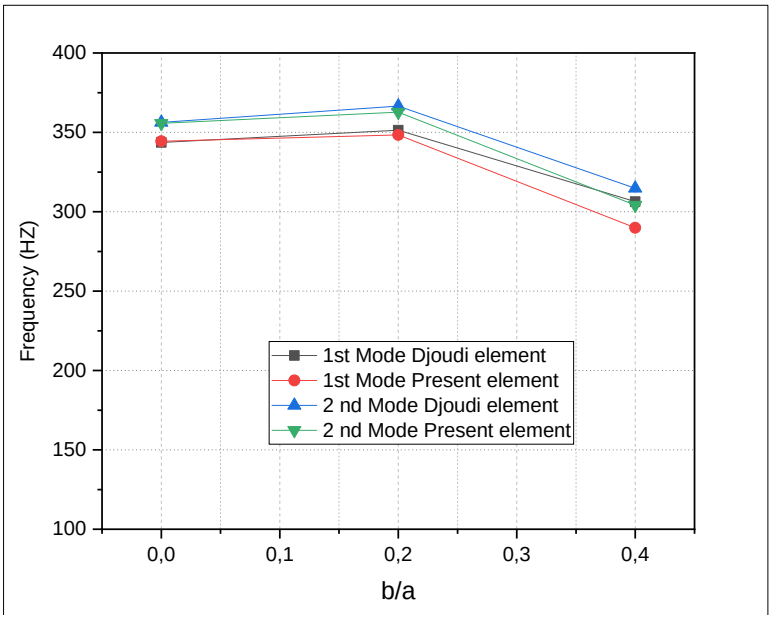

Figure 12. Comparison of natural frequencies against the size of the hole for a clamped panel

4. Conclusions

A three-node triangular cylindrical shell element is proposed using assumed strains and the deep shell theory. This element has only external degrees of freedom, three translations, and two rotations at each corner node. The displacement field of the developed element is calculated by integrating the assumed strain functions that satisfy the compatibility equations. The numerical integration is used for the evaluation of the element stiffness and mass matrices. The performance and accuracy of the developed element have been verified with various numerical examples in static and free vibration of cylindrical structures. The following advantages can be concluded from the numerical results of the current element:

- In comparison to elements containing internal nodes, such as the nine-node element, this element is simpler, with simply corner nodes and the five necessary exterior degrees of freedom;
- It has a rapid convergence rate to the exact solutions for static and free vibration analyses;
- The triangular shape of this element is more advantageous than the quadrilateral form because it facilitates meshing when the geometric domain of the structure is complicated;
- High accuracy and good performance have been obtained using the present element with only coarse meshes.

The results of this triangular cylindrical shell element show monotonic convergence and are in excellent accord with the analytical solutions and the results of various elements available in the literature. In perspective, this element can be applied to functionally graded shells, composite shell materials, and non-linear problems of shell structures.

5. Declarations

5.1. Author Contributions

Conceptualization, H.S.; methodology, H.S., L.B., A.B., F.B., and L.F.; writing—preparation of the original draft, H.S. and L.B.; writing—editing and editing, H.S., L.B., A.B., F.B., and L.F. All authors have read and agreed to the published version of the manuscript.

5.2. Data Availability Statement

The data presented in this study are available in the article.

5.3. Funding

The authors received no financial support for the research, authorship, and/or publication of this article.

5.4. Conflicts of Interest

The authors declare no conflict of interest.

6. References

[1] Yang, H. T. Y., Saigal, S., Masud, A., & Kapania, R. K. (2000). A survey of recent shell finite elements. International Journal for Numerical Methods in Engineering, 47(1–3), 101–127. doi:10.1002/(SICI)1097-0207(20000110/30)47:1/3<101::AID-NME763>3.0.CO;2-C.

[2] Zienkiewicz, O. C. (1967). The Finite Element Method in Structural and Continuum Mechanics: Numerical Solution of Problems in Structural and Contimuum Mechanics. McGraw-Hill, New York City, United States.

[3] Liang, Y., & Izzuddin, B. A. (2022). Locking-free 6-noded triangular shell elements based on hierarchic optimization. Finite Elements in Analysis and Design, 204, 103741. doi:10.1016/j.finel.2022.103741.

[4] Abed-Meraim, F., & Combescure, A. (2007). A physically stabilized and locking-free formulation of the (SHB8PS) solid-shell element. European Journal of Computational Mechanics, 16(8), 1037–1072. doi:10.3166/REMN.16.1037-1072.

[5] Trinh, V. D., Abed-Meraim, F., & Combescure, A. (2011). A new assumed strain solid-shell formulation "SHB6" for the six-node prismatic finite element. Journal of Mechanical Science and Technology, 25(9), 2345–64. doi:10.1007/s12206-011-0710-7.

[6] Batoz, J. -L, & Tahar, M. Ben. (1982). Evaluation of a new quadrilateral thin plate bending element. International Journal for Numerical Methods in Engineering, 18(11), 1655–1677. doi:10.1002/nme.1620181106.

[7] Yang, H. T. Y., Saigal, S., & Liaw, D. G. (1990). Advances of thin shell finite elements and some applications-version I. Computers and Structures, 35(4), 481–504. doi:10.1016/0045-7949(90)90071-9.

[8] Dagade, V. A., & Kulkarni, S. D. (2022). Static and free vibration analysis of sandwich shell panels using quadrilateral flat shell finite element. Materials Today: Proceedings, 63, 295–301. doi:10.1016/j.matpr.2022.03.084.

[9] Jones, R. E., & Strome, D. R. (1966). Direct stiffness method analysis of shells of revolution utilizing curved elements. AIAA Journal, 4(9), 1519–1525. doi:10.2514/3.3729.

[10] Connor, J. J., & Brebbia, C. (1967). Stiffness Matrix for Shallow Rectangular Shell Element. Journal of the Engineering Mechanics Division, 93(5), 43–65. doi:10.1061/jmcea3.0000894.

[11] Cantin, G., & Clough, R. W. (1968). A curved, cylindrical-shell, finite element. AIAA Journal, 6(6), 1057–1062. doi.org/10.2514/3.4673.

[12] Koziey, B. L., & Mirza, F. A. (1997). Consistent thick shell element. Computers and Structures, 65(4), 531–549. doi:10.1016/S0045-7949(96)00414-2.

[13] Dawe, D. J. (1975). High-order triangular finite element for shell analysis. International Journal of Solids and Structures, 11(10), 1097–1110. doi:10.1016/0020-7683(75)90089-X.

[14] Cowper, G. R., Lindberg, G. M., & Olson, M. D. (1970). A shallow shell finite element of triangular shape. International Journal of Solids and Structures, 6(8), 1133–1156. doi:10.1016/0020-7683(70)90052-1.

[15] Kim, Y. H., Jones, R. F., & Lee, S. W. (1990). Study of 20-node solid element. Communications in Applied Numerical Methods, 6(3), 197–205. doi:10.1002/cnm.1630060306.

[16] Ayad, R., Zouari, W., Meftah, K., Zineb, T. Ben, & Benjeddou, A. (2013). Enrichment of linear hexahedral finite elements using rotations of a virtual space fiber. International Journal for Numerical Methods in Engineering, 95(1), 46–70. doi:10.1002/nme.4500.

[17] Belounar, L., & Guenfoud, M. (2005). A new rectangular finite element based on the strain approach for plate bending. Thin-Walled Structures, 43(1), 47–63. doi:10.1016/j.tws.2004.08.003.

[18] Belounar, A., Benmebarek, S., Houhou, M. N., & Belounar, L. (2019). Static, free vibration, and buckling analysis of plates using strain-based Reissner–Mindlin elements. International Journal of Advanced Structural Engineering, 11(2), 211–230. doi:10.1007/s40091-019-0226-4.

[19] Belounar, A., Benmebarek, S., & Belounar, L. (2020). Strain based triangular finite element for plate bending analysis. Mechanics of Advanced Materials and Structures, 27(8), 620–632. doi:10.1080/15376494.2018.1488310.

[20] Belounar, A., Benmebarek, S., Houhou, M. N., & Belounar, L. (2020). Free Vibration with Mindlin Plate Finite Element Based on the Strain Approach. Journal of the Institution of Engineers (India): Series C, 101(2), 331–346. doi:10.1007/s40032-020-00555-w.

[21] Boussem, F., Belounar, A., & Belounar, L. (2022). Assumed strain finite element for natural frequencies of bending plates. World Journal of Engineering, 19(5), 620–631. doi:10.1108/WJE-02-2021-0114.

[22] Boussem, F., & Belounar, L. (2020). A Plate Bending Kirchhoff Element Based on Assumed Strain Functions. Journal of Solid Mechanics, 12(4), 935–952. doi:10.22034/jsm.2020.1901430.1601.

[23] Belounar, A., Boussem, F., & Tati, A. (2022). A Novel C_0 Strain-Based Finite Element for Free Vibration and Buckling Analyses of Functionally Graded Plates. Journal of Vibration Engineering and Technologies, 0123456789. doi:10.1007/s42417-022-00577-x.

[24] Belounar, A., Boussem, F., Houhou, M. N., Tati, A., & Fortas, L. (2022). Strain-based finite element formulation for the analysis of functionally graded plates. Archive of Applied Mechanics, 92(7), 2061–2079. doi:10.1007/s00419-022-02160-y.

[25] Belounar, A., Belounar, L., & Tati, A. (2022). An Assumed Strain Finite Element for Composite Plates Analysis. International Journal of Computational Methods. doi:10.1142/s0219876222500347.

[26] Belarbi, M. T., & Maalem, T. (2005). On improved rectangular finite element for plane linear elasticity analysis. Revue Europeenne des Elements, 14(8), 985–997. doi:10.3166/reef.14.985-997.

[27] Bouzidi, L., Belounar, L., & Guerraiche, K. (2019). Presentation of a new membrane strain-based finite element for static and dynamic analysis. International Journal of Structural Engineering, 10(1), 40–60. doi:10.1504/IJSTRUCTE.2019.101431.

[28] Fortas, L., Belounar, L., & Merzouki, T. (2019). Formulation of a new finite element based on assumed strains for membrane structures. International Journal of Advanced Structural Engineering, 11, 9–18. doi:10.1007/s40091-019-00251-9.

[29] Ram, A. K., & Mohanty, S. (2021). Experimental investigation on dynamic behavior of silt-rich fly ash using cyclic triaxial and bender element tests. Innovative Infrastructure Solutions, 6(4), 1-24. doi:10.1007/s41062-021-00582-1.

[30] Barrera, C. S., & Tardiff, J. L. (2022). Static and dynamic properties of eggshell filled natural rubber composites for potential application in automotive vibration isolation and damping. Journal of Cleaner Production, 353, 131656. doi:10.1016/j.jclepro.2022.131656.

[31] Belounar, L., & Guerraiche, K. (2014). A new strain based brick element for plate bending. Alexandria Engineering Journal, 53(1), 95–105. doi:10.1016/j.aej.2013.10.004.

[32] Guerraiche, K. H., Belounar, L., & Bouzidi, L. (2018). A new eight nodes brick finite element based on the strain approach. Journal of Solid Mechanics, 10(1), 186–199.

[33] Khiouani, H. E., Belounar, L., & Houhou, M. N. (2020). A new three-dimensional sector element for circular curved structures analysis. Journal of Solid Mechanics, 12(1), 165–174. doi:10.22034/jsm.2019.1867106.1430.

[34] Messai, A., Belounar, L., & Merzouki, T. (2019). Static and free vibration of plates with a strain based brick element. European Journal of Computational Mechanics, 1–21. doi:10.1080/17797179.2018.1560845.

[35] Ashwell, D. G., & Sabir, A. B. (1972). A new cylindrical shell finite element based on simple independent strain functions. International Journal of Mechanical Sciences, 14(3), 171–183. doi:10.1016/0020-7403(72)90074-4.

[36] Djoudi, M. S., & Bahai, H. (2003). A shallow shell finite element for the linear and non-linear analysis of cylindrical shells. Engineering Structures, 25(6), 769–778. doi:10.1016/S0141-0296(03)00002-6.

[37] Djoudi, M. S., & Bahai, H. (2004). A cylindrical strain-based shell element for vibration analysis of shell structures. Finite Elements in Analysis and Design, 40(13–14), 1947–1961. doi:10.1016/j.finel.2003.11.008.

[38] Djoudi, M. S., & Bahai, H. (2004). Strain based finite element for the vibration of cylindrical panels with openings. Thin-Walled Structures, 42(4), 575–588. doi:10.1016/j.tws.2003.09.003.

[39] Bourezane, M. (2017). An efficient strain based cylindrical shell finite element. Journal of Solid Mechanics, 9(3), 632–649.

[40] Timoshenko, S., & Woinowsky-Krieger, S. (1959). Theory of plates and shells. McGraw-hill, New York, United States.

[41] Macneal, R. H., & Harder, R. L. (1985). A proposed standard set of problems to test finite element accuracy. Finite Elements in Analysis and Design, 1(1), 3–20. doi:10.1016/0168-874x(85)90003-4.

[42] Sabir, A. B., & Lock, A. C. (1972). A curved, cylindrical shell, finite element. International Journal of Mechanical Sciences, 14(2), 125–135. doi:10.1016/0020-7403(72)90093-8.

[43] Lindberg, G.M., Olson, M.D. & Cowper, E.R. (1969). New Developments in the Finite Element Analysis of Shells. National Research Council of Canada, Quarterly Bulletin of the Division of Mechanical Engineering and the National Aeronautical Establishment, 4, 1-38.

[44] ASabir, A. B., & Charchaechi, T. A. (1982). Curved rectangular and general quadrilateral shell finite elements for cylindrical shells. The math of finite element and application, 231-239.

[45] Soedel, W. (2004). Vibrations of shells and plates. CRC Press, Boca Raton, United States. doi:10.4324/9780203026304.

[46] Lim, C. W., & Liew, K. M. (1995). A higher order theory for vibration of shear deformable cylindrical shallow shells. International Journal of Mechanical Sciences, 37(3), 277–295. doi:10.1016/0020-7403(95)93521-7.

[47] Petyt, M. (1971). Vibration of curved plates. Journal of Sound and Vibration, 15(3), 381–395. doi:10.1016/0022-460X(71)90432-9.

[48] Kanok-nukulchai, W. (1979). A simple and efficient finite element for general shell analysis. International Journal for Numerical Methods in Engineering, 14(2), 179–200. doi:10.1002/nme.1620140204.

[49] Huang, H. C., & Hinton, E. (1986). A new nine node degenerated shell element with enhanced membrane and shear interpolation. International Journal for Numerical Methods in Engineering, 22(1), 73–92. doi:10.1002/nme.1620220107.

[50] Lee, S. J., & Han, S. E. (2001). Free-vibration analysis of plates and shells with a nine-node assumed natural degenerated shell element. Journal of Sound and Vibration, 241(4), 605–633. doi:10.1006/jsvi.2000.3313.

Appendix I

The 15×15transformation matrix [C] for the present element SBTDS is given as:

$$[C]=\begin{bmatrix} P_1(x_1,\varphi_1,y_1) \\ P_2(x_2,\varphi_2,y_2) \\ P_3(x_3,\varphi_3,y_3) \end{bmatrix} \quad \text{A-1}$$

and the 3×15 matrix [P_i] evaluated from Equation 8 is as follows:

$$\left[P_{(x_i,\varphi_i,y_i)}\right]=\begin{bmatrix} 0 & R\cos\varphi_i & 0 & R\sin\varphi_i & 1 & 0 & x_i & 0 & y_i & 0 & 0 & 0 & 0 & 0 & -Ry_i \\ \sin\varphi_i & x\sin\varphi_i & -\cos\varphi_i & -x\cos\varphi_i & 0 & 1 & 0 & 0 & 0 & 0 & 0 & 0 & Ry_i & \frac{y_i^2}{2} & Rx_i \\ -\cos\varphi_i & -x\cos\varphi_i & -\sin\varphi_i & -x\sin\varphi_i & 0 & 0 & 0 & R & 0 & -\frac{x_i^2}{2} & -\frac{x_i^3}{6} & -\frac{y_i x_i^3}{6R} & -R^2 & -Ry_i & 0 \\ 0 & 0 & 0 & 0 & 0 & -\frac{1}{R} & 0 & 0 & 0 & 0 & 0 & -\frac{x_i^3}{6R} & -y_i & -\left(R+\frac{y_i^2}{2R}\right) & -x_i \\ 0 & -\cos\varphi_i & 0 & -\sin\varphi_i & 0 & 0 & 0 & 0 & 0 & -x_i & -\frac{x_i^2}{2} & -\frac{y_i x_i^2}{2R} & 0 & 0 & 0 \end{bmatrix} \quad \text{A-2}$$

where (x_i, φ_i, y_i), (i=1, 2, 3) are the coordinates of the three-element node.